Mem. S.A.It. Vol. 77, 711

Memorie della

Evolutionary paths for galaxies and AGNs:

new insights by the Spitzer space telescope

A. Franceschini[1], G. Rodighiero[1], S. Berta[1] and P. Cassata[1,2]

[1] Dipartimento di Astronomia – Universita' di Padova, Vicolo Osservatorio 2, I-35122 Padova, Italy, e-mail: franceschini@pd.astro.it
[2] IASF/INAF, Milano

Abstract. We compare the history of the galaxy mass build-up, as inferred from near-IR observations, and the Star Formation Rate of massive stars in the comoving volume traced by deep extensive far-IR surveys, both possible now with the Spitzer Space Telescope. These two independent and complementary approaches to the history of galaxy formation consistently indicate that a wide interval of cosmic epochs between $z \sim 0.7$ to ~ 2 brackets the main evolutionary phases. The rate of the integrated galaxy mass growth indicated by the IR-based comoving SFR appears consistent with the observed decrease of the stellar mass densities with redshift. There are also indications that the evolution with z of the total population depends on galaxy mass, being stronger for moderate-mass, but almost absent up to $z = 1.4$ for high-mass galaxies, thus confirming previous evidence for a "downsizing" effect in galaxy formation. The most massive galaxies appear already mostly in place by $z \sim 1$.
Although a precise matching of this galaxy build-up with the growth of nuclear supermassive black-holes is not possible with the present data (due to difficulties for an accurate census of the obscured AGN phenomenon), some preliminary indications reveal a similar mass/luminosity dependence for AGN evolution as for the hosting galaxies.

Key words. Galaxies: elliptical and lenticular, cD – Galaxies: spiral – Galaxies: irregular – Infrared: general – Infrared: galaxies – Cosmology: observations

1. Introduction

The cosmological origin of the galaxy morphological sequence can now be very effectively constrained by the wide IR multi-wavelength coverage offered by the Spitzer Space Telescope, including the near-IR photometric imaging by the IRAC and the far-IR imaging by the MIPS instruments. By combining these with the unique imaging capabilities of HST/ACS and the enormous photon-collecting power of spectrographs on large ground-based telescopes (VLT, Keck), we have now a definite chance to directly picture *in-situ* the process of galaxy formation.

The latter has remained a rather controversial issue untill recently. Published results from high redshift galaxy surveys appear not unfrequently in disagreement with each other (see Faber et al. 2005 for a recent review). This is partly due to the small sampled ar-

Send offprint requests to: A. Franceschini

eas and the corresponding substantial field-to-field variance. However, a more general problem stems from the apparent conflict between reports of the detection of massive galaxies at very high redshifts (e.g. Cimatti et al. 2004; Glazebrook et al. 2004) and indications for a fast decline in the comoving number density at $z > 1$ (e.g. Franceschini et al. 1998; Fontana et al. 2004).

The most direct way of constraining the evolutionary history of galaxies and trying to resolve these discrepancies is to derive the redshift-dependent stellar mass functions from deep unbiased surveys (e.g. Bundy, Ellis & Conselice 2005). We contribute to this effort by exploiting in this paper very deep public imaging by the GOODS project to select a complete sample of high-z ($z \leq 2$) galaxies selected in the 3.6 μm IRAC near-IR band. Near-IR surveys are best suited for the study of faint high-redshift galaxy populations, for various reasons. Compared to UV-optical selection, the observed fluxes are minimally affected by dust extinction. At the same time they are good indicators of the stellar mass content of galaxies (Dickinson et al. 2003; Berta et al. 2004), and closer to provide a mass-selection tool. For typical spectra of evolved galaxies, the IRAC channel also benefits by a K-correction particularly favourable for the detection of high-redshift galaxies.

In addition to the Spitzer observations, the GOODS and related CDFS projects have provided the community with an unprecedented amount of high quality optical and near-IR data in CDFS, particularly the very deep multi-band ACS imaging, allowing the most accurate morphological analysis currently possible. We will illustrate here the power of combining such multi-wavelength information in the analysis of the evolutionary mass and luminosity functions of faint galaxies.

A complementary view on galaxy formation is possible by direct sampling the rate of star formation based on suitable tracers. As established by exploratory observations with ISO and SCUBA (e.g. Franceschini et al. 2001; Elbaz et al. 2002; Smail et al. 2002), most accurate SFR determinations require the detection of dust emission in the far-IR, which often includes the majority of the radiant energy by massive stars. Our direct estimates of the evolutionary stellar mass functions are then compared with the most updated results on the comoving density of star formation by Spitzer far-IR observations. Modulo an assumption about the stellar initial mass function, the two approaches provide the complementary integral and differential views of star formation, respectively.

Galaxy formation has involved a variety of complex phenomena (see e.g. Baugh et al. 2005), including tidal interactions and merging, black-hole formation, accretion, and feedback processes. The ubiquitous presence of super-massive black-holes in galaxy nuclei (Magorrian et al. 1998) and the relevant observed scaling laws (Ferrarese and Merritt, 2000) suggest that feedback by nuclear activity (Springel et al. 2005) might have had an important influence on the process. This motivates us in looking also for comparison with the evolutionary patterns in the Active Galactic Nuclei population.

We adopt a standard cosmology (Ω_M=0.3, $\Omega_\Lambda = 0.7$) and express the H_0 dependence in terms of $h \equiv H_0/100\ Km/s/Mpc$.

2. Cosmic Evolution of the Galaxy Mass and Luminosity Functions

Of the two approaches to the history of galaxy formation – the one based on the study of the instantaneous SFR with suitable indicators, and the other estimating the evolutionary stellar mass functions – the latter has been recently recognized to benefit by various advantages (e.g. much lower extinction uncertainties) and to be more robust.

The evolution of the galaxy stellar mass function has been recently studied by us using a multi-wavelength dataset in the Chandra Deep Field South (CDFS) area, obtained from GOODS (Dickinson et al. 2004) and other projects (VVDS, Le Fevre et al. 2004), and including very deep high-resolution imaging by HST/ACS. Our reference catalogue of faint high-redshift galaxies, which we have thoroughly tested for completeness and reliability, comes from a deep ($S_{3.6} \geq 1$ μJy) image by

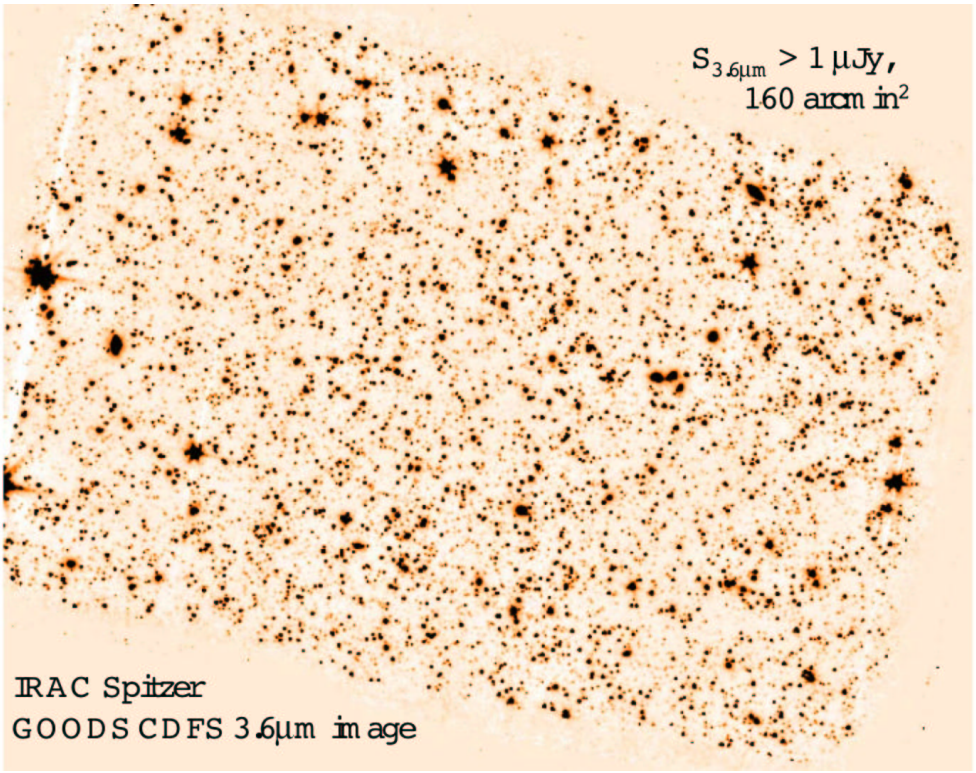

Fig. 1. Image at 3.6 μm of the GOODS region in the CDFS. The area covered is 12×18 square arcminutes approximately and the exposure time per sky pointing was 23 hours as a minimum. The image sensitivity is better than 1 μJy for point sources. 5622 sources with $S_{3.6\mu} > 1\mu Jy$ are detected inside the Spitzer/ACS common area of 160 sq. arcmin, 5302 of which are galaxies and 320 stars.

IRAC on the Spitzer Observatory (see Figure 1). These data are complemented with extensive optical spectroscopy by the ESO FORS2 and VIMOS spectrographs, while deep K-band VLT/ISAAC imaging is also used to derive further complementary statistical constraints and to assist the source identification and SED analysis. We have selected a highly reliable IRAC 3.6μm sub-sample of 1478 galaxies with $S_{3.6} \geq 10$ μJy, 47% of which have spectroscopic redshift, while for the remaining objects both COMBO-17 and *Hyperz* are used to estimate the photometric redshift.

Based on this extensive dataset, we have estimated time-dependent galaxy luminosity and stellar mass functions, while luminosity/density evolution is further constrained with the number counts and redshift distributions. The deep ACS imaging allows us to differentiate these evolutionary paths by morphological type, which can be reliably performed at least up to $z \sim 1.5$ for the two main early- (E/S0) and late-type (Sp/Irr) classes.

These data, as well as our direct estimate of the stellar mass function above $M_* h^2 = 10^{10} M_\odot$ for the spheroidal subclass, consistently evidence a progressive dearth of such objects to occur starting at $z \sim 0.7$, paralleled by an increase in luminosity. A similar trend, with a more modest decrease of the mass function, is also shared by spiral galaxies, while the irregulars/mergers show a positive evolution (increased number) up to $z \simeq 1.5$.

It is interesting to note that the decrease of the comoving density with redshift of the total population appears to depend on galaxy mass,

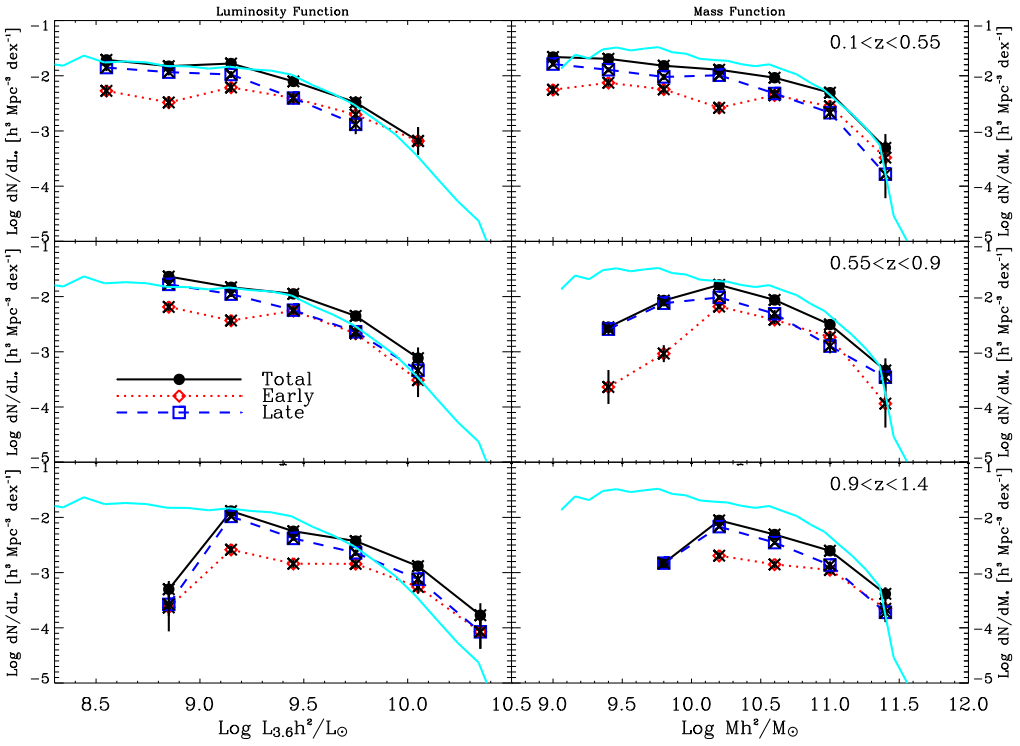

Fig. 2. Mass (*right-hand panels*) and luminosity (*left-hand panels*) function estimates derived from the 3.6 μm IRAC/GOODS sample with $S_{3.6}$ >10 μJy, splitted into three redshift bins from $z = 0.1$ up to $z = 1.4$. The contributions of the various morphological classes is marked with different symbols: early-types (open diamonds - dotted lines), late-types (open squares - dashed lines), total (filled circles - solid lines). The thin solid line on the right marks the local mass function from Cole et al. (2001).

being stronger for moderate-mass, but almost absent until $z = 1.4$ for high-mass galaxies, thus confirming previous evidence for a "downsizing" effect in galaxy formation (e.g. Cowie et al. 1996).

3. Probing the Evolution of the Comoving Star Formation Rate with Far-IR Observations

The usual way of determining the star formation activity in high-redshift galaxies is based on optical observations of the UV rest-frame flux (Lilly et al. 1995; Madau et al. 1996; Le Fevre et al. 2004). However, it has become recently evident that a probably major fraction of the emission by the most massive, luminous and short-lived stars, during the stage when they are still embedded inside their parent dusty molecular clouds, is optically extinguished and reprocessed at wavelengths from the mid-IR to the sub-millimeter.

3.1. The ISO and SCUBA explorations

The Infrared Space Observatory mission and the SCUBA/JCMT observations have offered the first tools for systematic cosmological surveys at long wavelengths. The good imaging capabilites of ISO have been exploited for deep mid-IR observations with sensitivities sufficient to detect sources at cosmological redshifts (Elbaz et al. 1999, 2002; Franceschini et al. 2001). Surveys in the wide band at 12-18μm

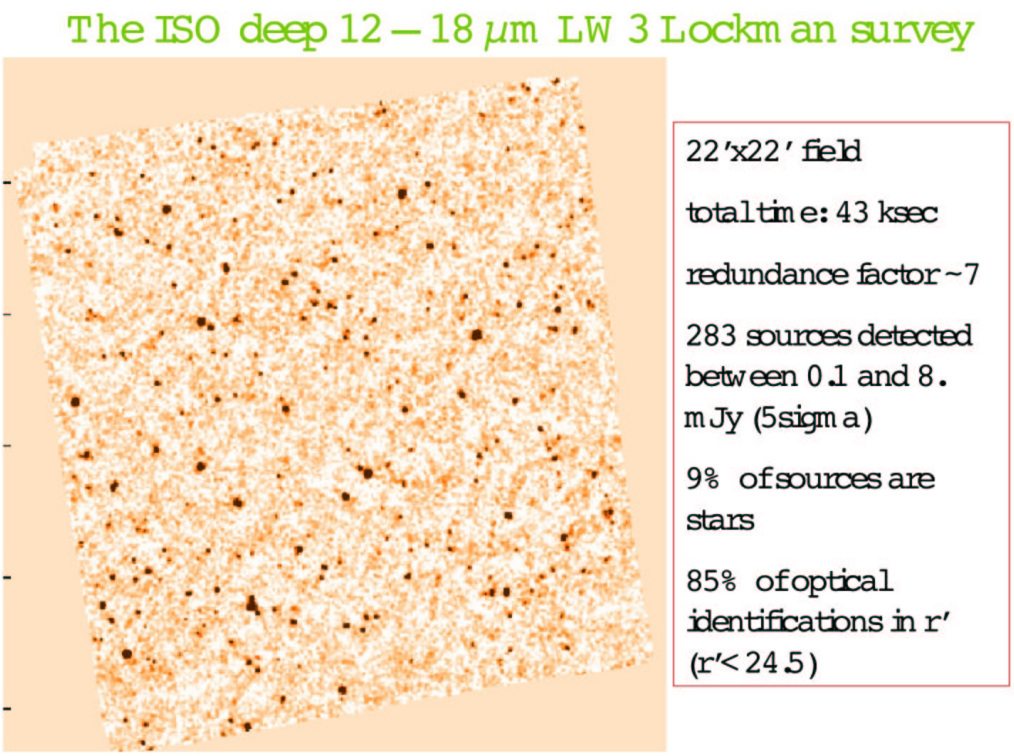

Fig. 3. Image at 15 μm of an area of 22x22 arcmins in the Lockman Hole by Rodighiero et al. (2004). Details about the observations are reported in the figure.

(λ_{eff} = 15 μm) have been performed in the ISOCAM GT, over a total area of 1.5 square degrees, with >1000 sources detected (Elbaz et al. 1999). Rodighiero et al. (2004) and Fadda et al. (2004) report a deep and a shallow survey of the Lockman Hole. An image of the deep field is reported in Figure 3. The two Hubble Deep Field areas (North and South, total of ~ 50 sq. arcmin) have been deeply surveyed at 15 μm down to 100 μJy (Rowan-Robinson et al. 1997; Aussel et al. 1998). At brighter fluxes, ELAIS has observed a total of 12 square degrees at 15 μm (Oliver et al. 2000; Vaccari et al. 2005).

The differential 15μm counts of extragalactic sources revealed a sudden upturn at S_{15} < 3 mJy, and a later convergence below S_{15} ~ 0.3 mJy (Elbaz et al. 1999; Gruppioni et al. 2003). These counts, far in excess of the no-evolution predictions, required strong evolution of the galaxy luminosity functions. At the faintest mid-IR fluxes, the redshift distributions of the ISO galaxy population showed an excess number of luminous sources between

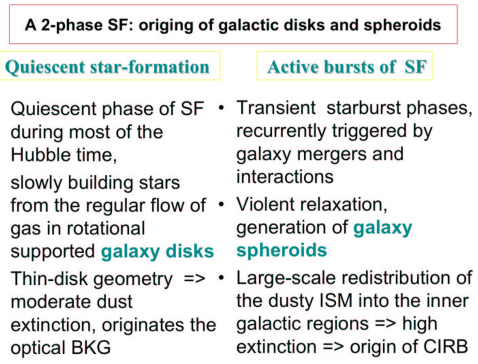

Fig. 4. A two-phase scheme for the evolution of galaxies selected in the optical and the IR.

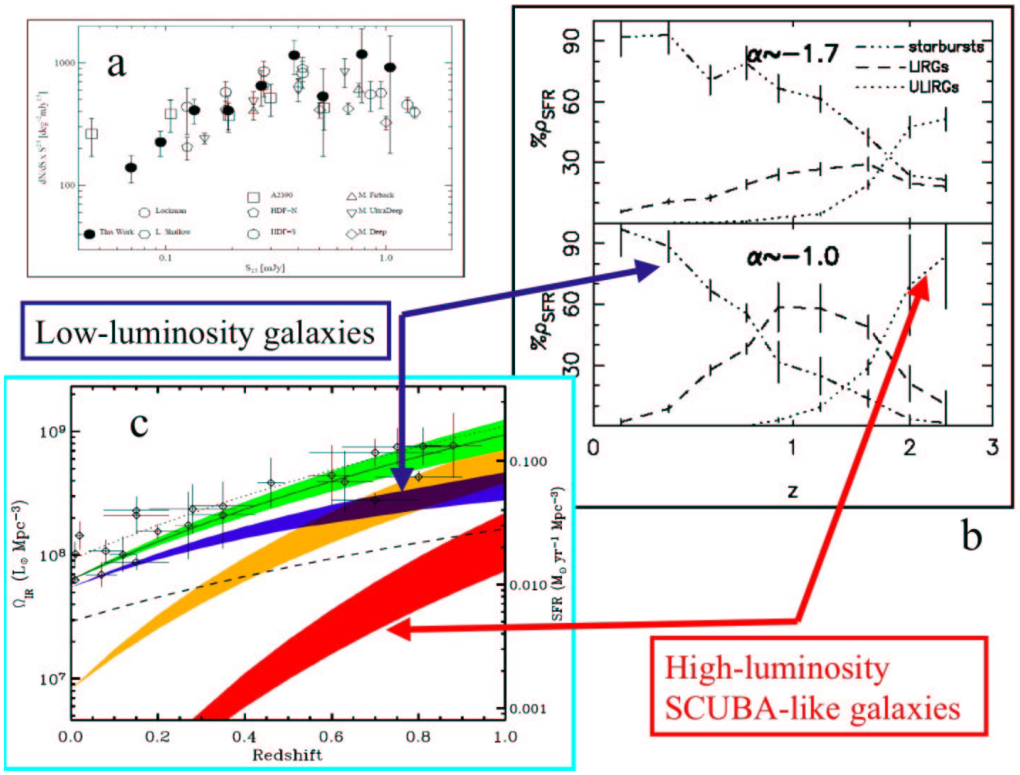

Fig. 5. *Panel a*: comparison of the differential 15 μm galaxy counts measured by ISO and Spitzer (Teplitz et al. 2005), showing excellent agreement. *Panel b*: relative contribution of low luminosity starbursts ($L_{IR} < 10^{11}\ L_{\odot}$), IR luminous sources (LIRGs, $L_{IR} > 10^{11}$) and ULIRGs ($L_{IR} < 10^{11}$) to the total SFR density of the universe as a function of redshift (Perez-Gonzales et al. 2005). *Panel c*: evolution of the comoving IR galaxy emissivity up to z=1 (green region) and the respective contributions from low luminosity galaxies ($L_{IR} < 10^{11}$, blue), IR luminous sources ($L_{IR} > 10^{11}$, orange) and ULIRGs ($L_{IR} < 10^{11}$, red).

z=0.5 and z=1. The upper redshift boundary is due to the ISOCAM mid-IR camera responsivity, implying a strong K-correction penalty for $z > 1$.

These results have been analyzed by Franceschini et al. (2001) and Elbaz et al. (2002) in conjunction with data and limits on the integrated sky intensity between 1 and 1000 μm set by COBE observations (the CIRB background), and with the sub-mm galaxy counts at 850 μm by SCUBA (see review by Smail et al. 2002). The combined multi-wavelength constraints imply that the far-IR volume emissivity of galaxies increases strongly from local to redshift $z \sim 1$ and should flatten or converge above. A comparison of the results of optical and IR cosmological surveys has been interpreted by Franceschini et al. (2001) to indicate that galaxies during their life form stars both in a quiescent mode, mostly responsible for the optical emission, and through short-lived starbursting episodes originating the far-IR emission, as summarized in Figure 4.

3.2. Results by the Spitzer Space Telescope

The far-IR imagers (MIPS and IRS) on Spitzer not only have confirmed the ISO results (Teplitz et al. 2005, see panel *(a)* in Figure 5), but, thanks to the longer wavelength capabilities of the 24 μm channel, have been able to ex-

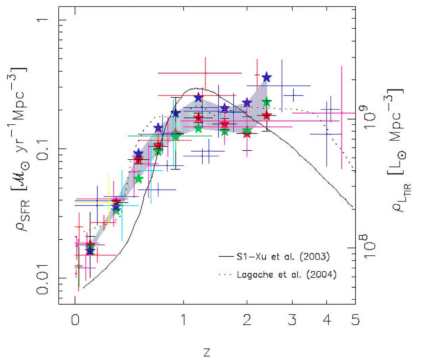

Fig. 6. Evolution of the comoving IR luminosity density and SFR as a function of redshift, taken from Perez-Gonzales et al. (2005). All values in the figure are computed for $h = 0.7$.

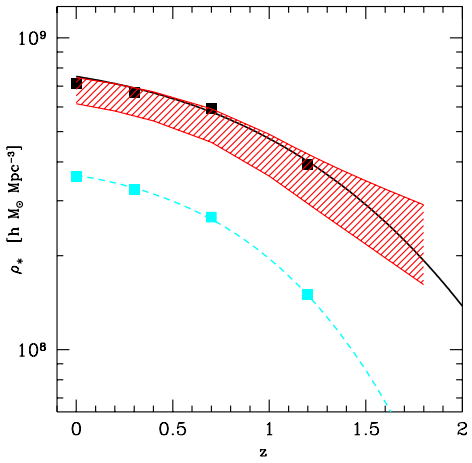

Fig. 7. The red-shaded area shows the expected evolution of the total integrated stellar mass density, as inferred from measurements of the comoving SFR. The upper datapoints and the continuous line are direct estimates by Franceschini et al. (2006) for the total galaxy population. The lower (cyan) points are the corresponding measurement for spheroidal galaxies, showing a somewhat faster convergence with z.

tend the ISO surveys to higher redshifts cover the critical redshift interval of $z \sim 1$ to ~ 2.

A region of the CDFS was observed at 24 μm by Le Floc'h et al. (2005) during the MIPS instrument GTO over a total area of 0.6 deg^2 and PSF FWHM of 6 arcsec. A sample of 2600 sources brighter than 80 μJy was combined with existing optical data in the field and used to derive bolometric IR luminosity functions and SFR's from z=0 to $\sim$ 1. These results imply that the comoving IR energy density of the Universe evolves like $(1 + z)^{3.9\pm0.4}$ up to $z \simeq 1$ (panel *(c)* in Fig. 5).

From MIPS 24 μm observations of the CDFS and HDFN, complemented with a systematic photometric redshift analysis exploiting the Spitzer IRAC data, Perez-Gonzales et al. (2005) confirm on one side the fast increase of the comoving SFR density to $z = 0.8$. As shown in Figure 6, the SFR density is found to continue rising from $z \sim 0.8$ to 1.2 with a smaller slope, but then to remain roughly constant above, in quite good agreement with results by Franceschini et al. (2001).

4. Discussion

It is of interest to verify how consistent the results about the redshift evolution of the integrated comoving stellar mass density $\rho_M(z)$ in Fig. 2 and the integrated star formation rate $\rho_{SFR}(z)$ in Fig. 6 are. Both quantities are based on the assumption of a universal Salpeter-like stellar IMF. The relationship of the two is simply:

$$\rho_M(z) = \rho_M(0) - \int_0^z \rho_{SFR}(z) \frac{dt}{dz} dz \qquad (1)$$

where $\rho_{SFR}(z) \simeq 0.014\ h\ (1 + z)^{3.9}$ at $z < 1$ and constant above (from Perez-Gonzales et al.), and where we can approximate $dt/dz = 1/[H_0(1 + z)^{2.5}]$. Assuming $\rho_M(0) \simeq (6.8 \pm 0.8)10^8\ h\ M_\odot/Mpc^3$ from Fukugita et al. (1998), we derive the evolution of the integrated stellar density reported as red shaded region in Figure 7. This is compared with the direct estimates by Franceschini et al. (2006) for the total galaxy population (suitably scaled from their fig.19 to correct for the different mass boundary). Within the large uncertainties, we see here that the two complementary views of the history of star formation appear to provide consistent results, hence in broad agreement with the assumed Salpeter IMF.

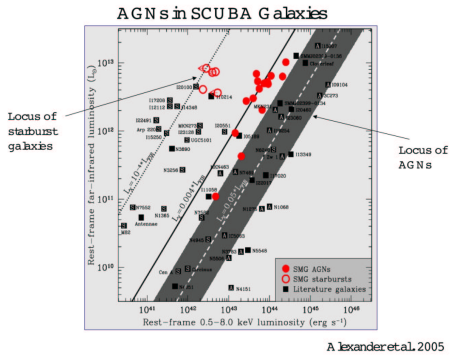

Fig. 8. Relation of far-IR to X-ray luminosity in high-z SCUBA galaxies (from Alexander et al. 2005). The bulk of these (red circles) are found to require both starburst and AGN simultaneous emissions.

Panels *(b)* and *(c)* in Fig. 5 also reveal some interesting features in the z-evolution of the SFR density as a function of the galaxy luminosity. Low-luminosity sources display their main SF activity below $z = 1$, while the highest-L ULIRGs develop their main activity phases at $z > 1.5$. Intermediate luminosity objects peak at intermediate redshifts of 0.7 to 1.5. This, together with the results illustrated in Fig. 2, provide concordant evidence that the formation and evolution of galaxies has been a strong function of luminosity and mass, as anticipated and discussed by various authors (Cowie et al. 1996, Franceschini et al. 1998, 1999; Treu et al. 2005).

Various attempts have been proposed to explain this effect, which seems to indicate a sort of inversion in the process of dynamical assembly of galaxies compared to the hierarchical expectation. One possibility considers energy feedback by a nuclear AGN stopping gas accretion and star formation in the most massive systems at high-z (Granato et al. 2004; Springel et al. 2005), while leaving it undisturbed in the lower mass galaxies where AGN activity is irrelevant.

This interpretation would call for a close relationship of the evolutionary histories of star-formation and nuclear Black Hole Accretion in AGNs. Unfortunately, a precise matching of galaxy build-up and the growth of nuclear super-massive black-holes is not possible with the present data, due to difficulties for an accurate census of the obscured AGN phenomenon. The problem has not yet been finally settled by the inclusion of data by the Spitzer surveys, bacause even a detailed IR multi-wavelength coverage is not sufficient to identify the whole of the obscured AGN population (see Franceschini et al. 2005; Polletta et al. 2006).

Preliminary results, mostly from X-ray surveys, confirm on one side that AGN and starburst activity occur concomitant in luminous high-z forming galaxies (as shown e.g. in the remarkable outcome by Alexander et al. 2005 reported in Figure 8).

It is also interesting to note that a similar mass/luminosity dependence for AGN evolution as for the hosting galaxies (with fast evolution with cosmic time for the highest-L and deferred activity for the lower-L objects) has been found in the luminosity functions of type-1 AGNs derived from complete X-ray surveys by Hasinger et al. (2005).

References

Alexander, D. M., Bauer, F. E., Chapman, S. C., et al., 2005, ApJ, 632, 736
Baugh, C. M., et al., 2005, MNRAS, 356, 1191
Berta, S., Fritz, J., Franceschini, A., et al., 2004, A&A, 418, 913
Bundy, K., Ellis, R. S., Conselice, C. J., 2005, ApJ 625, 621
Cimatti A., Daddi E., Renzini A. et al., 2004, Nature, 430, 184
Cowie, L. L., Songaila, A., Hu, E. M., Cohen, J. G., 1996, AJ, 112, 839
Dickinson, M., Papovich, C., Ferguson, H.C., Budavari, T., 2003 ApJ, 587, 25
Dickinson, M., et al., 2004, American Astronomical Society Meeting 204, 2004 AAS 204, 3313
Elbaz, D., Cesarsky, C. J., Fadda, D., et al., 1999, A&A, 351, 37L
Elbaz, D., Cesarsky, C. J., Chanial, P., et al., 2002, A&A 384, 848
Faber, S., et al., 2005, astro-ph/0506044
Fadda, D., Lari, C., Rodighiero, G., et al., 2004, A&A, 427, 23

Ferrarese, L., & Merritt, D. 2000, ApJ, 539, L9
Fontana, A., Pozzetti, L., Donnarumma, I., et al. 2004, A&A, 424, 23
Franceschini, A., Silva, L., Fasano, G. et al., 1998, ApJ, 506, 600
Franceschini, A., Hasinger, G., Miyaji, T., Malquori, D., 1999, MNRAS 310, L5.
Franceschini, A. Aussel, H., Cesarsky, C., et al., 2001, A&A, 378, 1
Franceschini, A., Manners, J., Polletta, M., et al. 2005, AJ 129, 2074
Franceschini, A., Rodighiero, G., Cassata, P., et al., 2006, A&A in press
Fukugita, M., Hogan, C. J., & Peebles, P. J. E. 1998, ApJ, 503, 518
Glazebrook, K., Abraham, R. G., McCarthy, P. J., et al, 2004, Nature, 430, 181
Granato, G. L., De Zotti, G., Silva, L., et al, 2004, ApJ, 600, 580
Hasinger, G., Miyaji, T., Schmidt, M., 2005, MNRAS 441, 417
Le Fèvre, O., Vettolani, G., Paltani, S., et al., 2004, A&A 428, 1043L
Le Floc'h, E., Papovich, C., Dole, H., et al., 2005, ApJ 632, 169
Lilly, S. J., Tresse, L., Hammer, F., Crampton, D., & Le Fevre, O. 1995, ApJ, 455, 108
Madau, P., Ferguson, H. C., Dickinson, M. E., Giavalisco, M., Steidel, C. C., & Fruchter, A. 1996, MNRAS, 283, 1388
Magorrian, J., Tremaine, S., Richstone, D., et al., 1998, AJ, 115, 2285
Oliver, S., et al., 2000, MNRAS 316, 749
Perez-Gonzalez, P., Rieke, G. H., Egami, E., et al., 2005, ApJ 630, 82
Polletta, M.C., Wilkes, B., Siana, B., et al., 2006, ApJ in press
Rodighiero, G., Lari, C., Fadda, D., Franceschini, A., Elbaz, D., Cesarsky, 2004, A&A 427, 773
Rowan-Robinson, M., Mann, R.G., Oliver, S., et al., 1997, MNRAS 289, 490
Smail, I., Ivison, R. J., Blain, A. W., & Kneib, J. P., 2002, MNRAS, 331, 495
Springel, V., Di Matteo, T., Hernquist, L., 2005, MNRAS, 361, 776
Teplitz, H.I., et al., 2005, astro-ph/0507558
Treu, T., Ellis, R. S. Liao, T. X., et al., 2005, ApJ, 633, 174
Vaccari, M., Lari, C., Angeretti, L., et al., 2005, MNRAS 358 397